11th International Symposium on Turbulence and Shear Flow Phenomena (TSFP11)
Southampton, UK, July 30 to August 2, 2019

MODULATION OF ATTACHED EXACT COHERENT STATES UNDER SPANWISE WALL OSCILLATION

Qiang Yang
State Key Laboratory of Aerodynamics,
China Aerodynamics Research and Development Centre,
Mianyang, Sichuan, 621000, P. R. China
yangqiang@skla.cardc.cn

Yongyun Hwang
Department of Aeronautics,
Imperial College London,
London SW7 2AZ, U.K.
y.hwang@imperial.ac.uk

ABSTRACT

The drag reduction deterioration by spanwise wall oscillation control is explored in this study. When the outer scale motions are absent from the domain, the optimal wall oscillation period is fixed in wall units, *i.e.*, $T^+ \simeq 100$, in perfect agreement with the convection time scale of the near-wall structures. A set of wall-normal localised exact coherent states under the modulation of spanwise wall oscillation are obtained. The saddle-node point of the bifurcation curves move towards higher Reynolds numbers until $T^+ \sim 100$, beyond which the solution can not be continued. The drag reduction of wall oscillation on logarithmic exact coherent states is negligible at $T^+ \simeq 100$, and this is the same for logarithmic eddies in long but narrow domains. However, substantial drag reduction is still achievable for isolated logarithmic eddies at larger oscillation periods, and the optimal periods tend to scale in a domain width related time scale, *i.e.*, L_z/u_τ, which is consistent with the bursting period of minimum logarithmic attached eddies, *i.e.*, $2 \sim 3L_z/u_\tau$. As the spanwise wall oscillation control only target eddies at a single period, this might be one reason that the optimal oscillation period varies with Reynolds number.

INTRODUCTION

Spanwise wall oscillation can significantly reduce turbulent skin-friction (Jung *et al.*, 1992). In this near-wall control strategy, the wall oscillates with the following spanwise wall velocity W_w,

$$W_w = A\sin(\omega t) = A\sin(2\pi t/T), \qquad (1)$$

where, ω (or T) is the oscillation frequency (or period), A the amplitude, and t the time. At low Reynolds numbers, say $Re_\tau = 200$, the drag reduction, DR, defined as the relative change of skin-friction coefficient between uncontrolled and controlled cases, *i.e.*, $DR = (C_{f,0} - C_f)/C_{f,0} \times 100$, can be as much as 40 at optimal control parameters. However, this type of near-wall control was found to be less effective as the increase of Reynolds numbers (Choi *et al.*, 2002; Touber & Leschziner, 2012; Hurst *et al.*, 2014; Gatti & Quadrio, 2016).

The drag reduction mechanics is mostly argued to be the interaction between the Stokes layer induced by the spanwise wall oscillation and the turbulent coherent structures. At high Reynolds numbers, large scale motions (LSMs) and very large scale motions (VLSMs) in the logarithmic and outer regions emerge and modulate the near-wall small scale structures (Hutchins & Marusic, 2007), thus the near-wall control becomes less effective (Agostini & Leschziner, 2018). Based on this observation, researchers have started to investigate large scale controls (Abbassi *et al.*, 2017; Yao *et al.*, 2018).

With growing recent evidence supporting Townsend's attached eddy hypothesis (Townsend, 1976), it is understood that self-similar coherent structures in the form of attached eddies in the logarithmic region generate a large portion of skin-friction at high Reynolds numbers (de Giovanetti *et al.*, 2016), and they are self-sustained at each length scale (Hwang & Cossu, 2011; Hwang & Bengana, 2016). Therefore, an interesting question is how the near-wall control modulate these individual eddies? Very recently, Yang *et al.* (2019) identified a set of exact coherent states (ECSs), which remarkably resembles Townsend's individual attached eddies. These ECSs provide an ideal dynamical system for understanding turbulence, as well as its control (Li & Graham, 2007; Ibrahim *et al.*, 2019). In this study, we attempt to explore the drag reduction control by spanwise wall oscillation via this approach, and shed light on the drag reduction deterioration mechanism.

NUMERICAL SETUP

We run numerical simulations for turbulent channel flow with constant mass flow rate. To reduce the dimension of the system, we only consider the lower-half of the channel, with the symmetry boundary condition applied on the top, *i.e.*, $\partial u/\partial y = 0$, $v = 0$, $\partial w/\partial y = 0$ at $y = h$. The simulations are run with open source code `Diablo` (Bewley,

2014). In this solver, the streamwise and spanwise directions are discretised using Fourier series with $2/3$ dealiasing rule, whereas the wall-normal direction is discretised using second-order central difference. The time integration is performed semi-implicitly by combining the Crank-Nicolson method with a third-order Runge-Kutta method. The `Diablo` solver is further coupled with the Newton-Krylov-Hookstep method (Viswanath, 2007; Willis *et al.*, 2013) to search the ECSs, which are in the form of travelling wave solutions in the present study. The numerical continuation in the parameter space is performed using a psudo-arclength algorithm.

To find the attached exact coherent states with spanwise wall oscillation, the set of ECSs by Yang *et al.* (2019) is used as the initial field. In their case, the following shift-reflect symmetry is applied explicitly to favour 'sinuous-mode' streak instability,

$$[u,v,w,p](x,y,z) = [u,v,-w,p](x-L_x/2,y,-z). \qquad (2)$$

Under this symmetry, spatial homogeneous spanwise wall velocity vanishes and the spanwise wall oscillation can not achieve any control effect. Therefore, the shift-reflect symmetry condition (2) is relaxed for the search of ECS in the presence of flow control. The idea for searching travelling wave form ECS by Newton-Krylov-Hookstep method lies in minimising the relative error between an initial state and the state obtained via first time-stepping the initial state by an interval T_s, then spatially shifting it backward by $T_s c_x$ (here c_x is the streamwise convection velocity of ECS). For ECS searching without control, the choice of T_s is arbitrary. However, under spanwise wall oscillation control, the flow shows periodicity due to the presence of periodic wall motion, thus the time interval needs to satisfy $T_s = nT$, where n is an integer number. In the present study, we chose $n = 1$ or 2, and the psudo-arclength continuation is then performed by gradually increasing the spanwise wall velocity amplitude A^+ at a fixed oscillation period T^+. Once the first ECS with spanwise wall oscillation is obtained, then the parameter continuation in the Reynolds number is performed using the psudo-arclength algorithm.

Two Reynolds numbers (based on the centreline velocity of the laminar flow with same mass flow rate, U_{cl} and the half channel height, h) are studied for the attached eddies. One is $Re = 23550$, corresponding to $Re_\tau = 800$ (based on friction velocity, u_τ and the half channel height, h) for a full simulation, at which Reynolds number Hurst *et al.* (2014) has performed a parameter study for large domain spanwise wall oscillation control. Another one is $Re = 55000$, which gives a clear range of logarithmic eddies and the logarithmic states are obtained with a eddy viscosity model (Yang *et al.*, 2019). The effect of the spanwise wall oscillation amplitude A^+ on the drag reduction is monotonic, with a nearly saturated state for $A^+ > 12$ (Quadrio *et al.*, 2009), thus all the cases in this study target at $A^+ \simeq 12$. There is an optimal oscillation period for the control, *i.e.*, $T^+ \simeq 100$, but much larger oscillation periods are also considered for the control of logarithmic eddies. Details of the simulation parameters are listed in tables 1 and 2.

Table 1. Simulation parameters for near-wall ('W') and logarithmic ('L_i') structures. 'R' is reference case, and 'F' full simulation with control.

	Re	$(L_x \times L_y \times L_z)/h$	C_s	A^+	T^+
R	23550	$12 \times 1 \times 4$	0	0	0
F	23550	$12 \times 1 \times 4$	0	12	100
W	23550	$10 \times 1 \times 0.25$	0	12	$0 \sim 310$
L1	55000	$10 \times 1 \times 0.375$	0.30	12	$0 \sim 100$
L2	55000	$10 \times 1 \times 0.5$	0.32	12	$0 \sim 100$
L3	55000	$10 \times 1 \times 0.75$	0.35	12	$0 \sim 100$

Table 2. Simulation parameters for wall states.

	$(L_x \times L_y \times L_z)/h$	A^+	T^+
ECS1	$0.6 \times 1 \times 0.3$	12	$0 \sim 137$
ECS2	$0.8 \times 1 \times 0.4$	12	$0 \sim 117$
ECS3	$1.2 \times 1 \times 0.6$	$0 \sim 12$	$0 \sim 79$

RESULTS AND DISCUSSION

We first show an instantaneous visulisation of the near-wall streaks at $y^+ \simeq 15$ for cases 'R' and 'F' in figure 1. The half-domain large box simulation at $Re = 23550$ gives a friction Reynolds number of $Re_\tau \simeq 800$ as in full domain simulation (Hurst *et al.*, 2014). It is noticed that at this Reynolds number, the near-wall and outer structures are well separated, as can be seen that the near-wall small streaks are on top of the footprints of the VLSMs. Case 'F' with control parameters of $A^+ \simeq 12$, $T^+ \simeq 100$ has a drag reduction of $DR \simeq 25$, which is also inline with the full domain DNS result by Hurst *et al.* (2014). Two features are obvious for the controlled field. First, the near-wall streaks are tilted in spanwise direction by the Stokes layer at this particular wall oscillation phase. Second, the near-wall streaks are significantly smeared by the Stokes layer, while the footprints of the VLSMs still remain very strong, and to some extend, almost unchanged.

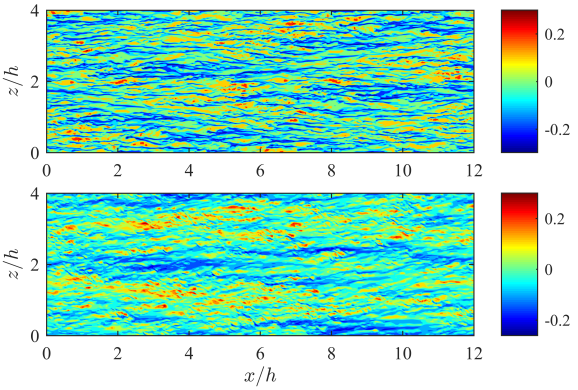

Figure 1. Streamwise velocity contour in xz plane of $y^+ \simeq 15$ for case 'R' (top) and case 'F' (bottom).

The second feature is even better supported by the one-dimensional pre-multiplied spanwise spectra of streamwise velocity shown in figure 2. Two energetic peaks are clearly visible: the inner one corresponding to the near-

wall streaks, the outer one corresponding to the VLSMs, and the linear ridge in-between corresponding to the logarithm structures. The outer peak penetrates deeply into the near-wall region, corresponding to the footprint effect. The spanwise wall oscillation significantly reduces the energy of the near-wall peak, while the outer peak and its penetration are only weakly modified. In the following, we focus on the control effect on near-wall and logarithmic states separately in scale isolated systems.

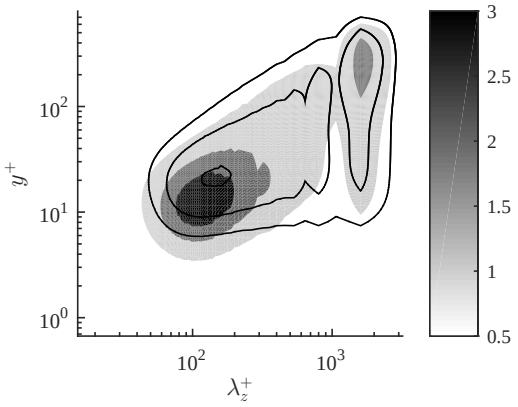

Figure 2. One-dimensional pre-multiplied spanwise spectra of streamwise velocity compared between case 'R' (shaded) and case 'F' (lines). u_τ of the uncontrolled case is used for both non-dimensionalisation.

Wall states

To study spanwise wall oscillation control on the near-wall structures only, we performance narrow domain simulations, *i.e.*, case 'W' with a series of oscillation periods T^+, at a fixed amplitude $A^+ \simeq 12$. The Reynolds number effect can be clearly seen in figure 3 with two Reynolds numbers, *i.e.*, $Re = 4725$ and 23550 taken from Hurst *et al.* (2014). At higher Reynolds number, the overall drag reduction is lower, with $DR_{max} \simeq 37$ at $Re = 4725$ and $DR_{max} = 28$ at $Re = 23550$. The optimal oscillation period scaled in inner units of the uncontrolled case is also lower, with $T^+_{opt} \simeq 100$ at $Re = 4725$ and $T^+_{opt} \simeq 80$ at $Re = 23550$. However, when narrow domain is considered for $Re = 23550$, the optimal oscillation period moves back to $T^+_{opt} \simeq 100$ again, perfectly in agreement with the low Reynolds number case. As the near-wall regeneration cycle bursts at a period of $T^+ \simeq 200 \sim 300$ (Flores & Jiménez, 2010), the optimal wall oscillation period is around the same order of such a bursting period. The narrow domain is only designed for the structure dynamics analysis, thus the predicted *DR* value is not accurate due to its artificial missing of large scale physics, which might be the reason that we see a big discrepancy in the *DR* values between narrow domain control at the high Reynolds number and large domain control at the low Reynolds number in figure 3.

As the exact coherent states form skeleton of turbulence, we then apply spanwise wall oscillation control on them. The bifurcation curves for 'ECS3' are displayed in figure 4 for different oscillation amplitudes at $T^+ \simeq 35$ (here the inner units are from the saddle-node point of the uncontrolled case). Spanwise wall oscillation can significantly alter the bifurcation curves, with the effect more ob-

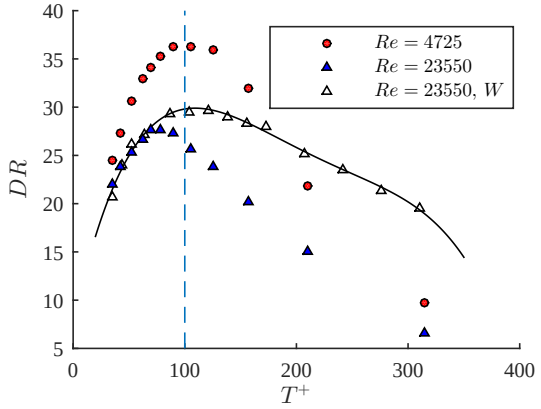

Figure 3. *DR* variation against oscillation periods (cases 'W'). The solid line is polynomial fitting.

vious on the upper branches than the lower ones, as also being found by Ibrahim *et al.* (2019) for blowing and suction control in Couette flow. The ECSs emerge at a critical Reynolds number via a saddle-node bifurcation, below which no such finite amplitude solution exists. It is clear that the control increases the critical Reynolds number, which indicates transition delay, or drag reduction for turbulence. Higher wall oscillation amplitude A^+ can better delay transition, and this trend is monotonic as in full domain DNS (Quadrio *et al.*, 2009).

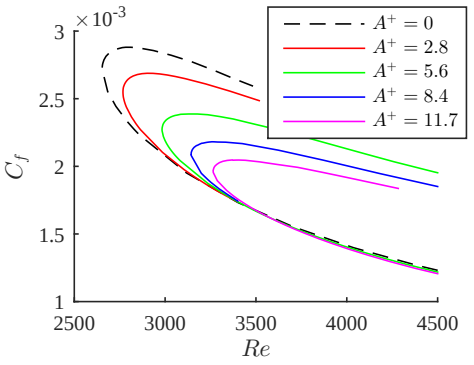

Figure 4. Bifurcation curves for 'ECS3' at $T^+ \simeq 35$.

The oscillation amplitude $A^+ \simeq 12$ is then chosen to study the effect of oscillation period T^+ for 'ECS1','ECS2' and 'ECS3'. For all the three ECSs, the oscillation period can only be extended up to $T^+ \sim 100$, above which the ECS with such a long period can not be converged. For $T^+ < 100$, the critical Reynolds number monotonically increases as oscillation period increases. Limited to the T^+ parameter range available, the critical Reynolds number reversal is not observed yet, but the upper and lower branches have become very close to each other at the largest T^+. This feature also reveals that the distance in C_f between the upper and lower branches of the uncontrolled case at a fixed Reynolds number can roughly give an estimation of the maximum drag reduction achievable. For instance, the estimated maximum *DR* values from 'ECS3', 'ECS2' and 'ECS1' are 35%, 25% and 20%, respectively. This is expected as the contribution to skin-friction from the wall state decreases as the Reynolds number increases (de Giovanetti *et al.*, 2016).

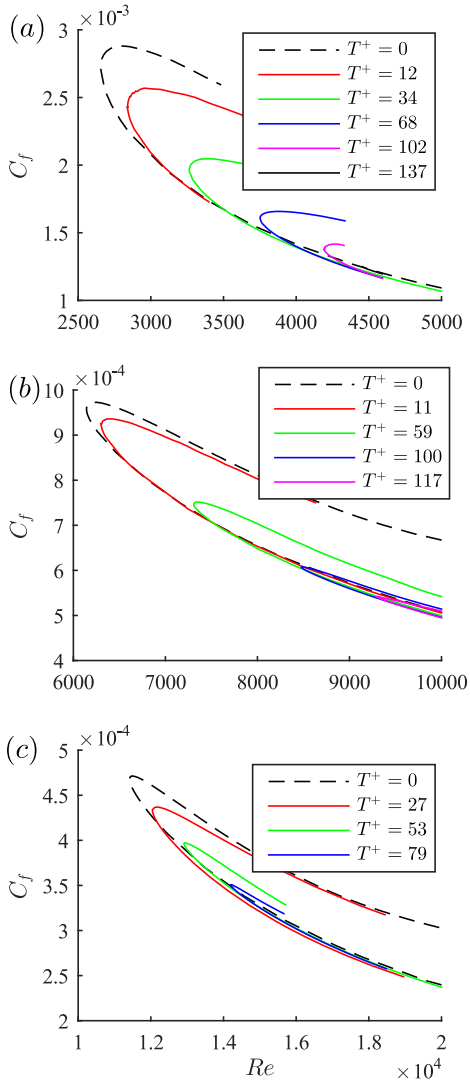

Figure 5. Bifurcation curves at $A^+ \simeq 12$ for (a) 'ECS3', (b) 'ECS2' and (c) 'ECS1'.

The visualisation of ECSs at $L_z/h = 0.3$ and $L_z/h = 0.6$ are shown in figure 6 for both uncontrolled and controlled cases at the lowest saddle-node points, *i.e.*, $T^+ = 79$ for $L_z/h = 0.3$ case, and $T^+ = 102$ for $L_z/h = 0.6$ case. As can be seen, spanwise wall oscillation does not alter the general shape of the ECSs, which are always featured by a streamwise meandering streak flanked by a pair of staggered vortices of alternating signs, forming the regeneration cycle. However, the controlled ECSs are pushed much further away from the wall compared to their uncontrolled counterparts, due to the Stokes layer, which is shown in figure 7(b) for $L_z/h = 0.3$ case at 8 equally separated phases during one oscillation period (circles in figure 7(a)). At this oscillation period, the Stokes layer of the ECS is in good agreement with the analytical solution of the laminar case. The unsteady Stokes layer also causes the unsteadiness of the ECS as expected, and we show the skin-friction variation for $L_z/h = 0.3$ case during one oscillation period as an example. The C_f oscillates at twice the frequency of the wall oscillation. However, this variation is just tiny.

The inner-scaled statistics are shown in figure 8 for $L_z/h = 0.6, 0.4$ and 0.3 cases with and without control. A general view is that, even inner-scaled, the near-wall peaks of the statistics are shifted away from the wall, and for

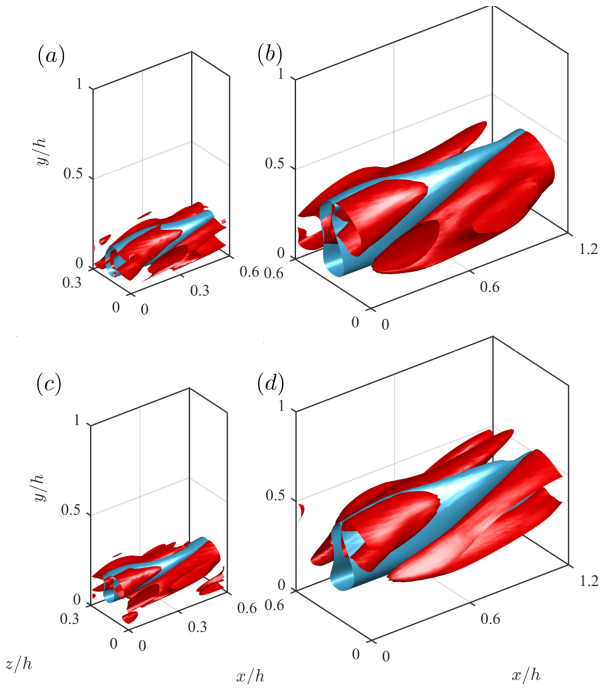

Figure 6. Exact coherent states at saddle-node points for (a,c) $L_z/h = 0.3$ and (b,d) $L_z/h = 0.6$: (a,b) uncontrolled cases; (c,d) controlled cases. The blue and red isosurfaces indicate $u'^+ = -2$ and $\lambda_2^+ = -0.002$, respectively.

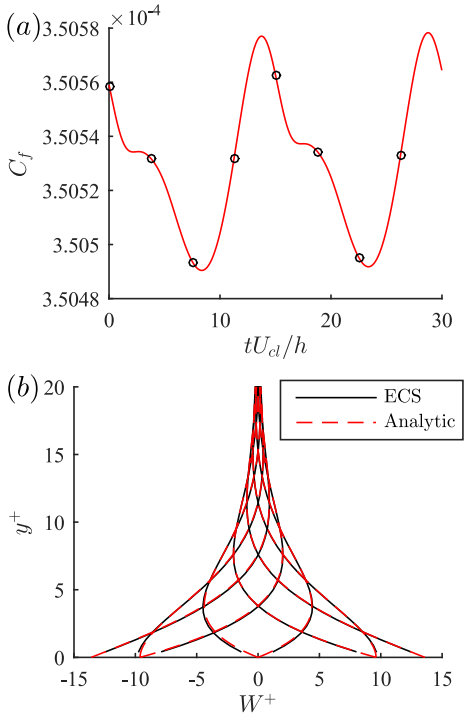

Figure 7. (a) C_f variation during one oscillation period for $L_z/h = 0.3$ controlled case; (b) the spanwise wall velocity profiles at 8 equally separated phases.

$L_z/h = 0.3$ case, this shifts are $\Delta y^+ \simeq 11$ for u^+_{rms}, $\Delta y^+ \simeq 10$ for v^+_{rms} and $\Delta y^+ \simeq 12$ for $-\overline{u'v'}^+$. This is quite similar to the 'virtual wall' in blowing and suction control (Chung & Talha, 2011), but here the 'virtual wall' is created by the Stokes layer.

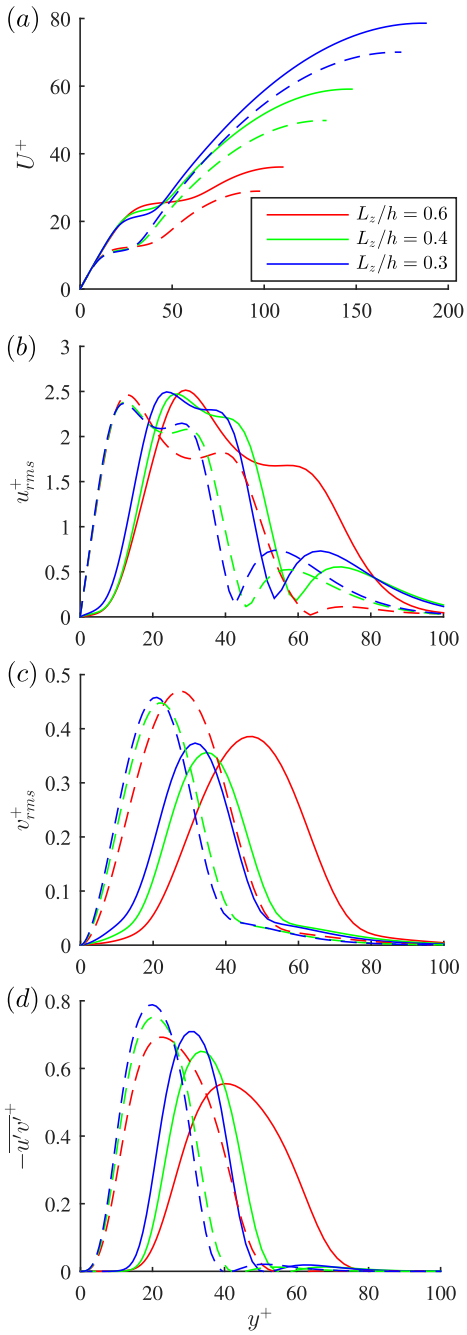

Figure 8. Statistics for wall states with control (solid lines) and without control (dashed lines): (a) U^+, (b) u^+_{rms}, (c) v^+_{rms} and (d) $-\overline{u'v'}^+$.

Logarithmic States

Spanwise wall oscillation is then applied to the logarithmic exact coherent states at $Re = 55000$, as identified by Yang *et al.* (2019) using over-elevated eddy viscosity. We extend the inner scale nature of wall states to the logarithmic states. The drag reduction results at $A^+ \simeq 12$ and $T^+ \simeq 100$ are listed in table 3, and a negligible drag reduction is observed. For 'ECSL3' case, there is even a drag increase. To understand the scaling nature of the logarithmic structures, we perform unsteady simulations in long but narrow domains, shown in table 1.

The logarithmic structures are visualised in figure 9, which are featured with long streaks (blue) and quasi-streamwise vortices (red) just as the ECSs. Different oscillation periods are considered for each logarithmic structure. The *DR* variation for each structure is shown in figure 10. At $T^+ \simeq 100$, drag reduction achievable is negligible as for the exact coherent states. However, a substantial drag reduction is still achievable for $T^+ \gg 100$. The optimal oscillation periods are not scaled in inner units, but in a domain width related time scale L_z/u_τ, which is around the same order of the bursting period of the logarithmic structures, *i.e.*, $2 \sim 3L_z/u_\tau$ (Hwang & Bengana, 2016). We note that the eddy viscosity approach used here is mainly to replace the effect of near-wall small eddies. The *DR* value from such a simple eddy viscosity model would definitely be less accurate compared to DNS result. Therefore, it is to be further investigated whether the same effect can also be observed in full DNS.

Table 3. Simulation parameters for logarithmic ECSs (upper branch) at $Re = 55000$, $A^+ \simeq 12$, $T^+ \simeq 100$.

	$(L_x \times L_y \times L_z)/h$	C_s	Re_τ	DR
ECSL1	$0.75 \times 1 \times 0.375$	0.30	789	0.5
ECSL2	$1.0 \times 1 \times 0.5$	0.32	989	2.8
ECSL3	$1.5 \times 1 \times 0.75$	0.35	1415	-0.7

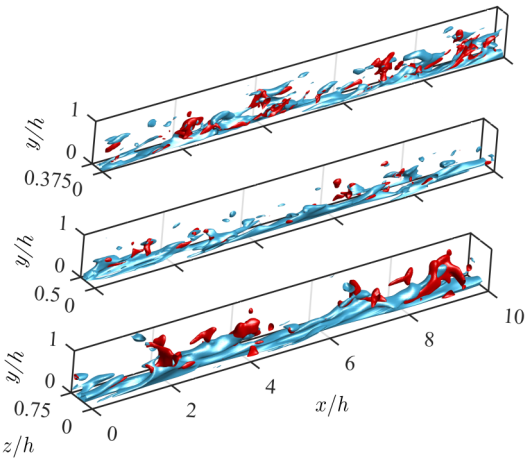

Figure 9. Logarithmic structures: top to bottom are 'L1', 'L2' and 'L3'. The blue and red isosurfaces indicate $u'^+ = -2$ and $v' = 1.5$, respectively.

CONCLUDING REMARKS

Spanwise wall oscillation is applied to isolated wall and logarithmic structures and their corresponding exact coherent states at high Reynolds numbers. Substantial drag reduction is achieved for both sates, but with different optimal oscillation periods. The wall states are optimally controlled at $T^+_{opt} \simeq 100$, but the logarithmic states at $T_{opt} \simeq L_z/u_\tau$, which are around the same order of the bursting periods of these states. This might make spanwise wall oscillation control challenging at high Reynolds number, since it only targets a single period. Recently, for DNS in a large domain, Yao *et al.* (2018) showed logarithmic structures can be con-

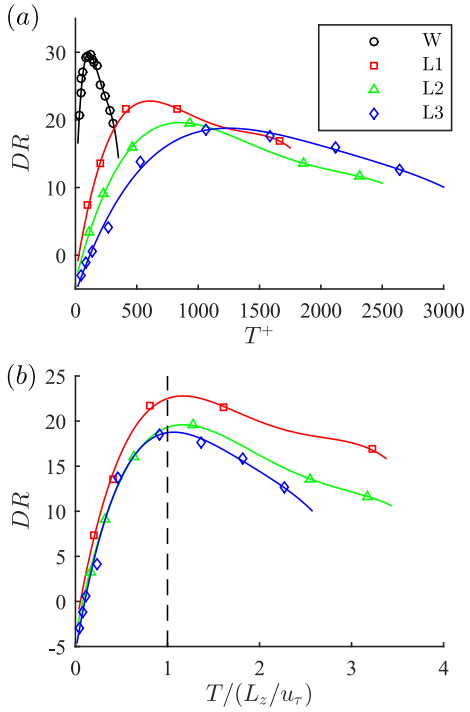

Figure 10. *DR* variation against oscillation periods at $A^+ \simeq 12$ for logarithmic structures: (a) inner and (b) bursting scaling. Solid lines are polynomial fitting.

trolled via spanwise opposed wall-jet forcing for drag reduction, and this result is consistent with the control of isolated logarithmic states in the present study. This is encouraging as near-wall based control might achieve a certain drag reduction at very high Reynolds numbers (Iwamoto *et al.*, 2005). Of course, in real situation, a hierarchy of attached eddies co-exist in the domain, and their non-linear interaction is not negligible (de Giovanetti *et al.*, 2016).

Another interesting finding probably is the drag reduction mechanism. What we have observed from the spanwise wall oscillation modulated ECSs is a wall-normal displacement of the coherent states, while the general feature of the state is still well maintained. A thicker sublayer is thus created, which is very similar to the so-called 'virtual wall' in blowing and suction control (Chung & Talha, 2011). It is worth further exploring what happens to the ECS at large oscillation periods ($T^+ \gg 100$) in the future.

ACKNOWLEDGEMENTS

This work was supported by the Natural Science Foundation of China (11802322) and the National Key Research and Development Program of China (2016YFA0401200). Q.Y. would like to thank Professor Y. M. Chung for initiating this work.

REFERENCES

Abbassi, M. R., Baars, W. J., Hutchins, N. & Marusic, I. 2017 Skin-friction drag reduction in a high-Reynolds-number turbulent boundary layer via real-time control of large-scale structures. *Int. J. Heat Fluid Fl.* **67**, 30–41.

Agostini, L. & Leschziner, M. 2018 The impact of footprints of large-scale outer structures on the near-wall layer in the presence of drag-reducing spanwise wall motion. *Flow Turbul. Combust.* **100** (4), 1037–1061.

Bewley, T. R. 2014 *Numerical Renaissance: simulation, optimization, & control*. San Diego: Renaissance Press.

Choi, J. I., Xu, C. X. & Sung, H. J. 2002 Drag reduction by spanwise wall oscillation in wall-bounded turbulent flows. *AIAA J.* **40** (5), 842–850.

Chung, Y. M. & Talha, T. 2011 Effectiveness of active flow control for turbulent skin friction drag reduction. *Phys. Fluids* **23** (2), 025102.

Flores, O. & Jiménez, J. 2010 Hierarchy of minimal flow units in the logarithmic layer. *Phys. Fluids* **22** (7), 071704.

Gatti, D. & Quadrio, M. 2016 Reynolds-number dependence of turbulent skin-friction drag reduction induced by spanwise forcing. *J. Fluid Mech.* **802**, 553–582.

de Giovanetti, M., Hwang, Y. & Choi, H. 2016 Skin-friction generation by attached eddies in turbulent channel flow. *J. Fluid Mech.* **808**, 511–538.

Hurst, E., Yang, Q. & Chung, Y. M. 2014 The effect of Reynolds number on turbulent drag reduction by streamwise travelling waves. *J. Fluid Mech.* **759**, 28–55.

Hutchins, N. & Marusic, I. 2007 Evidence of very long meandering features in the logarithmic region of turbulent boundary layers. *J. Fluid Mech.* **579**, 1–28.

Hwang, Y. & Bengana, Y. 2016 Self-sustaining process of minimal attached eddies in turbulent channel flow. *J. Fluid Mech.* **795**, 708–738.

Hwang, Y. & Cossu, C. 2011 Self-sustained processes in the logarithmic layer of turbulent channel flows. *Phys. Fluids* **23** (6).

Ibrahim, J. I., Yang, Q., Doohan, P. & Hwang, Y. 2019 Phase-space dynamics of opposition control in wall-bounded turbulent flows. *J. Fluid Mech.* **861**, 29–54.

Iwamoto, K., Fukagata, K., Kasagi, N. & Suzuki, Y. 2005 Friction drag reduction achievable by near-wall turbulence manipulation at high Reynolds numbers. *Phys. Fluids* **17** (1), 011702.

Jung, W. J., Mangiavacchi, N. & Akhavan, R. 1992 Suppression of turbulence in wall-bounded flows by high-frequency spanwise oscillations. *Phys. Fluids A* **4** (8), 1605–1607.

Li, W. & Graham, M. D. 2007 Polymer induced drag reduction in exact coherent structures of plane Poiseuille flow. *Phys. Fluids* **19** (8), 083101.

Quadrio, M., Ricco, P. & Viotti, C. 2009 Streamwise-travelling waves of spanwise wall velocity for turbulent drag reduction. *J. Fluid Mech.* **627**, 161–178.

Touber, E. & Leschziner, M. A. 2012 Near-wall streak modification by spanwise oscillatory wall motion and drag-reduction mechanisms. *J. Fluid Mech.* **693**, 150–200.

Townsend, A. A. 1976 *The structure of turbulent shear flow*. Cambridge University Press.

Viswanath, D. 2007 Recurrent motions within plane Couette turbulence. *J. Fluid Mech.* **580**, 339–358.

Willis, A. P., Cvitanovic, P. & Avila, M. 2013 Revealing the state space of turbulent pipe flow by symmetry reduction. *J. Fluid Mech.* **721**, 514–540.

Yang, Q., Willis, A. P. & Hwang, Y. 2019 Exact coherent states of attached eddies in channel flow. *J. Fluid Mech.* **862**, 1029–1059.

Yao, J., Chen, X. & Hussain, F. 2018 Drag control in wall-bounded turbulent flows via spanwise opposed wall-jet forcing. *J. Fluid Mech.* **852**, 678–709.